LANGMUIR

High-Density Protein Loading on Hierarchically Porous Layered Double Hydroxide Composites with a Rational Mesostructure

Yasuaki Tokudome,[*,†] Megu Fukui,[†] Naoki Tarutani,[†] Sari Nishimura,[†] Vanessa Prevot,[‡,§] Claude Forano,[‡,§] Gowsihan Poologasundarampillai,[∥] Peter D. Lee,[∥] and Masahide Takahashi[†]

[†]Department of Materials Science, Graduate School of Engineering, Osaka Prefecture University, Sakai, Osaka 599-8531, Japan

[‡]Institut de Chimie de Clermont-Ferrand (ICCF), Université Clermont Auvergne, Université Blaise Pascal, BP 10448, F-63000 Clermont-Ferrand, France

[§]Institut de Chimie de Clermont-Ferrand (ICCF), UMR 6296, Centre National de la Recherche Scientifique (CNRS), F-63171 Aubiere, France

[∥]School of Materials, The University of Manchester, Oxford Road, Manchester M13 9PL, United Kingdom

S *Supporting Information*

ABSTRACT: Hierarchically porous biocompatible Mg−Al−Cl-type layered double hydroxide (LDH) composites containing aluminum hydroxide (Alhy) have been prepared using a phase-separation process. The sol−gel synthesis allows for the hierarchical pores of the LDH−Alhy composites to be tuned, leading to a high specific solid surface area per unit volume available for high-molecular-weight protein adsorptions. A linear relationship between the effective surface area, S_{EFF}, and loading capacity of a model protein, bovine serum albumin (BSA), is established following successful control of the structure of the LDH−Alhy composite. The threshold of the mean pore diameter, D_{pm}, above which BSA is effectively adsorbed on the surface of LDH−Alhy composites, is deduced as 20 nm. In particular, LDH−Alhy composite aerogels obtained via supercritical drying exhibit an extremely high capacity for protein loading (996 mg/g) as a result of a large mean mesopore diameter (>30 nm). The protein loading on LDH−Alhy is >14 times that of a reference LDH material (70 mg/g) prepared via a standard procedure. Importantly, BSA molecules pre-adsorbed on porous composites were successfully released on soaking in ionic solutions (HPO_4^{2-} and Cl^- aqueous). The superior capability of the biocompatible LDH materials for loading, encapsulation, and releasing large quantities of proteins was clearly demonstrated.
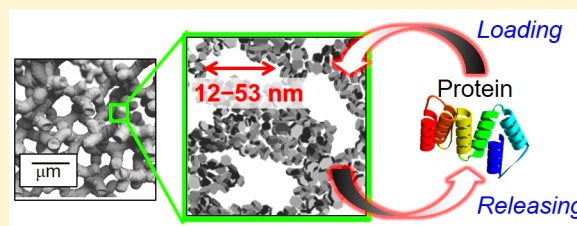
INTRODUCTION

Protein immobilization on solid surfaces is of relevance to a wide range of research areas, with potential applications in biotechnology and physiology.[1] The activity of immobilized proteins is an important consideration, which affects inorganic/bio interfacial properties, such as antifouling and antibacterial properties[2] and hemo-/biocompatibilities.[3] Various solids have been studied as supports for proteins,[1] including layered double hydroxides (LDHs), which are promising candidates as a result of their outstanding biocompatibility and an ability to limit denaturation of immobilized proteins.[4] The active conformation of proteins is retained on two-dimensionally flat and highly hydrophilic surfaces of LDHs,[5] to avoid denaturation, which otherwise takes place on curved inorganic surfaces.[6,7] As a result, heme proteins, which usually denature on inorganic solids, can be immobilized on LDH surfaces without losing their inherent activity. Immobilized heme proteins are currently used as bioelectrodes with high sensitivity.[8,9]

Synthesizing LDHs with meso-/macropores is highly promising to achieve high capacity loading of proteins. The rational design of the porous structure in the nanometer to sub-micrometer scale is especially important because micropores (<2 nm) and relatively small mesopores that typically adsorb ion/small molecules cannot accommodate large protein molecules (∼tens of nanometers in size). The surface area accessible by proteins (defined here as effective surface area, S_{EFF}) strongly depends upon the pore diameter, D_p, of porous LDHs. To date, LDHs of micrometer and sub-micrometer scale structures have been reported as particles,[10,11] sheets,[12] and plates with grooves;[13] however, increasing S_{EFF} is challenging and hard to achieve with these materials. This is because LDH crystals as building blocks used to assemble materials are relatively large, typically in sub-micrometers.[13,14] Limiting the dimensions of LDH crystals to nanoscale, assembling them into three-dimensional (3D) porous solids, and optimizing their meso- and macroporous structures remains a big challenge when attempting to maximize S_{EFF} and, thereby, protein loading. Recently, we have reported the preparation of monolithic LDHs with hierarchical pores.[15] The hierarchical pores of macro (1 μm) and meso (8 nm) formed
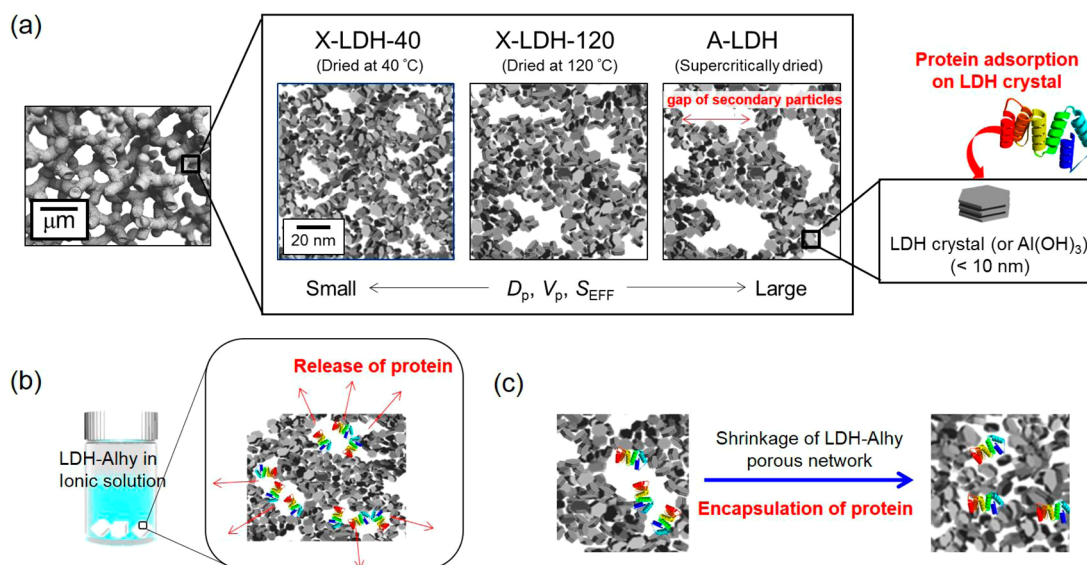
Figure 1. Schematic illustration depicting the research carried out in this study. (a) LDH nanocrystals and Alhy nanoparticles form biocompatible solids with hierarchically porous structures. (b) Pre-adsorbed proteins (BSA) released by soaking the composite in solutions containing competitive anionic adsorbates (HPO_4^{2-} and Cl^-). (c) Large shrinkage of mesoporous networks (length shrinkage of 50%) upon drying leading to successfully encapsulated BSA molecules.

spontaneously via a facile sol–gel reaction. It was also reported that target oxyanions (CrO_4^{2-}, SO_4^{2-}, MoO_4^{2-}, etc.) and small molecules diffuse rapidly through the macropores and adsorb on a large surface derived from the mesopores.[16] However, the development of LDHs with tens of nanometer pores, which are optimized to maximize S_{EFF} through structural hierarchy, is still needed to exploit the applications of biocompatible solid supports with a high capacity for protein loading.

We prepare here biocompatible composites of LDH and aluminum hydroxide (Alhy) with two levels of hierarchical tunable pores in the range of tens of nanometers and a few micrometers. Dependence of the mean mesopore diameter, D_{pm}, upon the synthesis parameters was investigated to tune the hierarchical porosity of the LDH–Alhy. Then, the adsorption of a large protein, bovine serum albumin (BSA), on the LDH–Alhy surfaces of various S_{EFF} was conducted to establish a relationship between S_{EFF} and loading capacity (Figure 1a). D_{pm} could be tuned from 12 to 53 nm, leading to a wide range of S_{EFF} for adsorption of BSA molecules. Particular interest was focused on aerogels obtained via supercritical drying,[17] on which considerable adsorption of the large protein molecules was achieved as a result of maximized S_{EFF}. Finally, the capability of the LDH–Alhy to release the immobilized protein in HPO_4^{2-} and Cl^- aqueous solutions was investigated (Figure 1b). The encapsulation as well as the release of BSA was attempted by inducing the shrinkage of the porous matrix after BSA loading (Figure 1c). The results demonstrated here provide key quantitative insights into protein loading on hydroxide-based biocompatible materials that display 14 times higher loading capacity than referential LDH materials.

■ EXPERIMENTAL SECTION

Chemical. Aluminum chloride hexahydrate ($AlCl_3 \cdot 6H_2O$, 98%) and magnesium chloride hexahydrate ($MgCl_2 \cdot 6H_2O$, 98%) were used as inorganic sources. A mixture of ultrapure water and ethanol (EtOH, 99.5%) was used as a solvent. (±)-Propylene oxide (PO, >99%) and isopropyl alcohol (IPA, 99.7%) were employed as a basic reagent and a liquid for sample washing, respectively. Poly(ethylene oxide) [PEO; viscosity average molecular weight (M_v) = 1 × 10⁶] was used as an

organic additive. Dipotassium hydrogen phosphate (K_2HPO_4, >99%), sodium chloride (NaCl, >99%), and hydrochloric acid (HCl, 36.0 wt %) were used to trigger desorption of BSA. PO, PEO, and BSA were purchased from Sigma-Aldrich Co., and all other reagents were from Wako Pure Chemicals Industries, Ltd. All chemicals were used as received. For comparison, reference LDH (Ref-LDH) was prepared by a standard pH constant co-precipitation approach[18] with a chemical composition of $[Mg_{0.68}Al_{0.32}(OH)_2Cl_{0.21}(CO_3^{2-})_{0.06} \cdot yH_2O]$. A commercial LDH [Com-LDH, $Mg_{0.75}Al_{0.25}(OH)_2(CO_3)_{0.125} \cdot 4H_2O$, Wako Pure Chemicals Industries, Ltd.] was purchased and used for further comparison.

Preparation of LDH–Alhy Xerogels and Aerogels. Typically, $AlCl_3 \cdot 6H_2O$ (1.58 g, 6.55 mmol), $MgCl_2 \cdot 6H_2O$ (1.06 g, 5.23 mmol), and various amounts (W_{PEO}) of grams of PEO were dissolved in a mixture of water/ethanol (4.00 mL/3.00 mL). PO (1.82 mL, 26.2 mmol) was added to this solution, maintained at 25 °C and stirred for 1 min, to yield a homogeneous sol. The sol was transferred to a polystyrene container, sealed, and kept at 40 °C. After 24 h, an opaque gel, thus obtained, was soaked in IPA for 1 h to exchange the water/ EtOH solvent that remained inside pores with IPA. This process was repeated at least 8 times with fresh IPA. Then, the gel was solvothermally treated in IPA at 180 °C for 24 h, followed by either ambient or supercritical drying. The ambient drying was performed at 40 and 120 °C in an oven to yield xerogels, named as "X-LDH-40" and "X-LDH-120", respectively. Supercritical drying was conducted with supercritical CO_2 (80 °C and 14.0 MPa), yielding aerogels, which are labeled as "A-LDH" in the following.

Structural Characterization. Fine structures of the samples were observed by field emission scanning electron microscopy (FE-SEM, S-4800, Hitachi, Japan). Crystal phases of the obtained samples were identified by X-ray diffraction (XRD, MultiFlex, Rigaku, Japan) using Cu Kα radiation (λ = 0.154 nm). Micro–mesoporous characters of the samples were investigated by a N_2 adsorption–desorption apparatus (BELSORP-mini II, Bel Japan, Inc., Japan). Prior to the measurement, the samples (A-LDH, X-LDH, Com-LDH, and Ref-LDH) were subjected to quick heat treatment to remove adsorbed water at 500 °C and then further outgassed under vacuum at 200 °C. The pore size distribution was calculated from the adsorption branch of the isotherm by the Barrett–Joyner–Halenda (BJH) method. The mean pore diameter, D_{pm}, and total pore volume, V_p (cumulative pore volume calculated from pores with D_p < 183 nm), were estimated from the distribution curves. The BJH method was also applied to assess partial
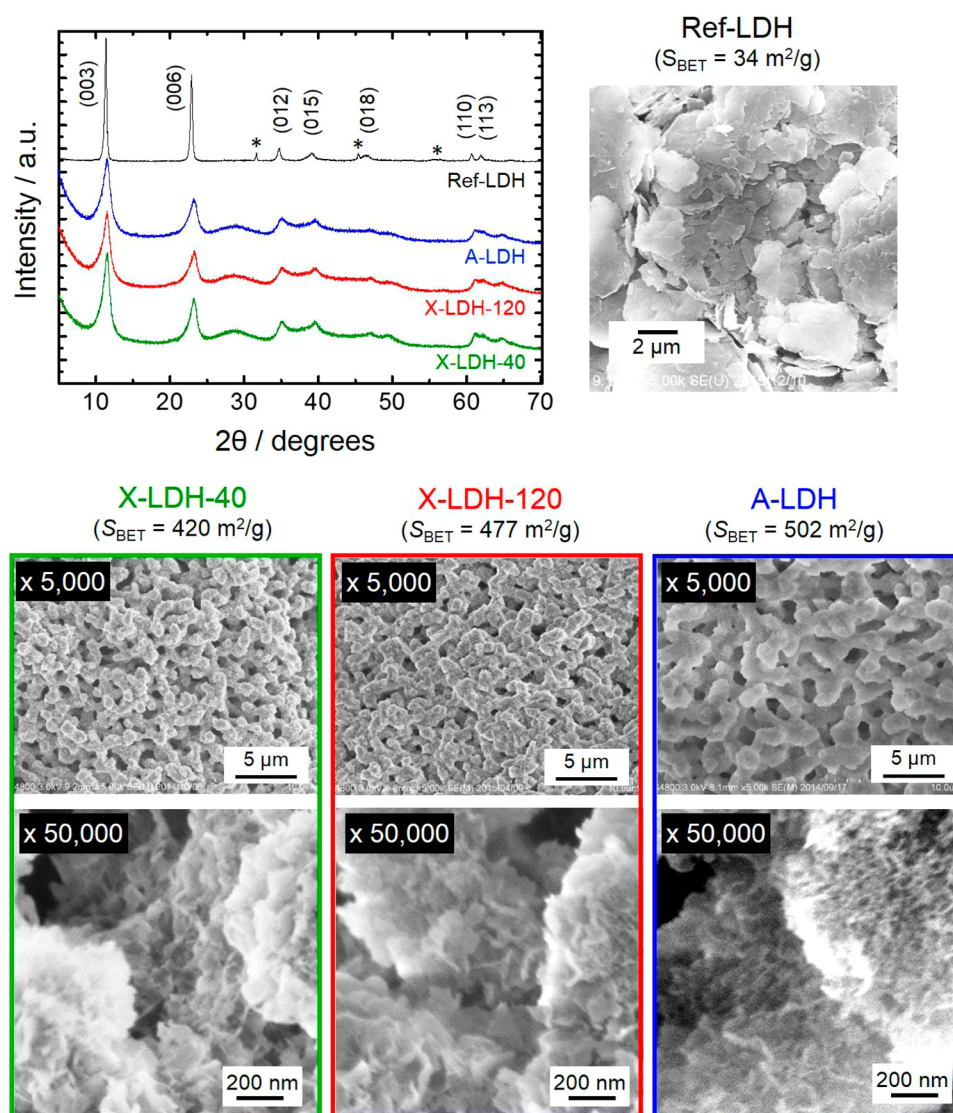
Figure 2. XRD patterns and FE-SEM images of Ref-LDH, X-LDH-40, X-LDH-120, and A-LDH [hydrotalcite, Joint Committee on Powder Diffraction Standards (JCPDS) 00-022-0700]. W_{PEO} = 0.03 g. (∗) Impurity NaCl phase.

specific surface area $[S_{(>x \, nm)}]$ derived from pores larger than a cutoff value. For example, $S_{(>5 \, nm)}$ corresponds to a specific surface area obtained by integrating surfaces of pores with $D_P > 5$ nm. The Brunauer−Emmett−Teller (BET) method was also applied to estimate the specific surface area, S_{BET}. Synchrotron X-ray micro-computed tomography (μ-CT) was employed to non-destructively obtain three-dimensional (3D) images of the drying process of the monoliths. A high-resolution synchrotron-based X-ray tomographic image was obtained from the Diamond-Manchester branchline I13-2 at Diamond Light Source.[19] The samples were kept at 300 K on the beamline using an in-house environmental stage.[20] A polychromatic filtered parallel-beam setup was used with a 0.81 μm effective pixel size and ∼2 μm spatial resolution. Over the 180° rotation, 3600 projections were collected at 0.05 s exposure time and tomographically reconstructed into a 3D volume using software developed at Diamond Light Source.[21] Visualization package Avizo was used to produce the 3D images and quantify shrinkage. The gel samples for the μ-CT measurements were prepared from AlCl$_3$·6H$_2$O (2.19 g), MgCl$_2$·6H$_2$O (0.553 g), W_{PEO} = 0.03 g, water (4.00 mL), ethanol (3.00 mL), and PO (2.27 mL).

BSA Sorption Test. Each of X-LDH (25 mg/mL), A-LDH (1.5 mg/mL), Ref-LDH (7.5 mg/mL), and Com-LDH [10 mg/mL, Mg$_6$Al$_2$(OH)$_{16}$CO$_3$·4H$_2$O, Wako Pure Chemicals Industries, Ltd.] was dispersed in aqueous BSA solutions of various concentrations (1.0−3.5

mg/mL) (the supporting note is in the Supporting Information). The mixtures were placed at 25 °C for 72 h. Supernatants of respective mixtures were collected through a membrane filter (0.45 μm) and analyzed by ultraviolet−visible (UV−vis) spectroscopy (V-670 spectrophotomater, JASCO Corp.). The concentration of BSA was estimated by the Beer−Lambert law using a peak intensity at 277.4 nm. The amount of adsorbed BSA was calculated from eq 1

$$C_s = \frac{(C_i - C_{eq})V}{m} \quad (1)$$

where C_s (mg/g) is the amount of BSA adsorbed by LDH-Alhy composites, C_i (mg/mL) and C_{eq} (mg/mL) are initial and equilibrium concentrations of BSA in the solution, respectively, V (mL) is the volume of the solution, and m (g) is the mass of LDH. The Freundlich equation (eq 2) was used as the isotherm model for BSA adsorption on the sample solids

$$\log C_s = \log K_f + \frac{1}{n_f} \log C_{eq} \quad (2)$$

where K_f (mg/g) is the Freundlich constant and n_f is the adsorption intensity. The BSA adsorption tests were conducted on LDH−Alhy composites prepared at W_{PEO} = 0, 0.01, 0.02, 0.03, and 0.04. To study BSA desorption, 30 mg of the sample, which had previously adsorbed

Table 1. Mesopore Characteristics of LDH−Alhy Composites

	X-LDH-40			X-LDH-120			A-LDH			Ref-LDH	Com-LDH
W_{PEO} (g)	0.02	0.03	0.04	0.02	0.03	0.04	0.02	0.03	0.04		
D_{pm} (nm)	14.1	14.1	12.3	19.9	16.9	15.5	53.2	40.8	38.1		
V_p (cm^3 g^{-1})	0.94	1.04	0.95	1.44	1.70	1.40	3.82	4.27	3.15		
S_{BET} (m^2 g^{-1})	390	420	389	394	477	397	397	502	380	34	123
$S_{(>2\ nm)}$ (m^2 g^{-1})	357	343	351	418	521	439	359	491	391	40	77

BSA in the solution of the BSA concentration of 2.5 mg/mL (25 °C for 72 h) was immersed in 0.1 M NaCl and 0.1 M K$_2$HPO$_4$ aqueous (25 °C for 72 h), respectively. The amounts of BSA molecules desorbed from A-LDH (W_{PEO} = 0.03 g) and Com-LDH were analyzed by the UV−vis technique. Some A-LDHs were dried after BSA adsorption (before the desorption test), and the effect of shrinkage on desorption was investigated. The reproducibility of adsorption isotherms was assessed on Com-LDH and X-LDH-40 (details in the Supporting Information).

■ RESULTS AND DISCUSSION

Synthesis of Hierarchically Porous LDH−Alhy with Tunable Porosities. The hierarchically porous LDH−Alhy composites were prepared via hydrolysis and condensation reactions of metal salts by alkalinization in the presence of PO according to our previously published method.[15] A nucleophilic attack of Cl$^-$ induces the ring-opening reaction of PO, and subsequent alkanization increases pH of the solution to precipitate LDHs.[22,23] This reaction process yields nanosized hydroxide particles (crystals) and leads to homogeneous gelation in 15 min as a result of a high degree of supersaturation generated in the reaction solution. The gelling solution phase separates[24] into a LDH−Alhy-rich solid phase and a PEO-rich fluid phase. Evaporative removal of the fluid phase leaves macropores (in the micrometer range). Simultaneously, the mesopores (in the nanometer range) were formed within the gel skeleton (Figure 1a). The mesopore size, D_p, and mesopore volume, V_p, which expectedly influence S_{EFF} and the adsorption capacity of proteins, varied as a function of W_{PEO} (the amount of PEO additive) and drying conditions.

Figure 2 shows XRD patterns and scanning electron microscopy (SEM) images of the different LDH−Alhy composites and Ref-LDH. The composites and Ref-LDH are ascribed to hydrotalcite-type LDH with typical powder X-ray diffraction (PXRD) patterns of a $R\bar{3}m$ hexagonal lattice.[25] Crystallite sizes estimated from Scherrer's equation using the (003) diffraction peak are 24 nm for Ref-LDH, 7.2 nm for X-LDH-40, 7.1 nm for X-LDH-120, and 6.8 nm for A-LDH. These values provide evidence that the crystallite sizes of X-LDH and A-LDH are comparable and far smaller than Ref-LDH used here as the reference, considered as a poorly crystallized material. Chemical analysis revealed that the LDH−Alhy composites have the composition of $[Mg_{0.66}Al_{0.33}(OH)_2Cl_{0.33-x}(CO_3^{2-})_{x/2} \cdot yH_2O] \cdot 2.0Al(OH)_3$. Alhy, which forms porous networks together with LDH crystals, displays a hydroxylated surface that is biocompatible with proteins, as confirmed by its use as an adjuvant in some vaccines.[26] As a result, the LDH−Alhy composites offer an extensive solid surface used for protein loading.

The LDH−Alhy composites produced here and Ref-LDH possess very different microstructures (Figure 2). The morphology of Ref-LDH is aggregates of LDH plates with the size of 1−4 μm. On the other hand, LDH−Alhy composites possess hierarchically porous structures with a monolithic form. As well as interconnected macropores with the pore diameter of

1−2 μm, mesopores are confirmed in the gel skeletons (higher magnification images in Figure 2). The difference of mesostructures is clearly supported by N$_2$ sorption measurements (Table 1). Large BET surface areas exceeding 400 m^2/g are derived from the mesoporosity, which are formed as interstices of constituent nanoparticles. The BJH pore size distributions of Ref-LDH, Com-LDH, and LDH−Alhy composites are plotted in Figures S1 and S2 of the Supporting Information. Com-LDH and Ref-LDH have negligible mesopores, whereas LDH−Alhy composites possess a considerable pore volume of 0.94−4.27 cm^3/g, originated from pores in the range of D_p < 150 nm. PEO changes the assembly of LDH and Alhy particles, and D_{pm} decreases with increasing W_{PEO} (Table 1). The formation of smaller mesopores with increasing W_{PEO} is caused by a decrease of the solvent, which is to be mesopores after drying in the LDH−Alhy-rich solid phase, leading to more packed LDH and Alhy crystallites.[27] The characteristics of mesopores also depends upon the drying conditions. A-LDHs possess the largest D_{pm} and V_p among the three sets of LDH−Alhy composites because the shrinkage is minimized by applying the supercritical drying.[17] To obtain better insight on the shrinkage upon the drying process of the monolithic LDHs, X-ray μ-CT was performed while the gels were left to dry at 300 K (Figure 3). Figure 3 shows 3D images of a small volume of the same gel before and after drying. It shows that shrinkage was isotropic, leading to a volume shrinkage of 85% and a linear shrinkage of 46%. The relatively large D_{pm} and V_p of X-LDH-120 compared to X-LDH-40 is due to a smaller degree of shrinkage upon drying. The faster drying at 120 °C forms cracks in the monolithic specimen and releases stress generated at the drying front, retarding isotropic shrinkage and leading to larger mesopores.[28] It should be emphasized again that X-LDH-40, X-LDH-120, and A-LDHs possess the identical chemical composition and crystallinity, and differences among these samples are only porosity in nanometer and micrometer scales. In summary, D_{pm} of LDH−Alhy composites was successfully tuned between 12 and 53 nm by the W_{PEO} value and drying conditions.

Effect of the Pore Structure on Protein Adsorption. The LDH−Alhy composites with various D_{pm} and V_p were assessed as bio-supports with a high capacity for protein loading. As an adsorbate, BSA was used, which is a large multi-domain protein with a hydrodynamic radius of 3.6 nm and 3D size of 5 × 7 × 7 nm^3.[29] Serum albumin, a major soluble constituent of the plasma proteins, has many physiological functions.[30] Moreover, BSA has been used as a model protein to investigate reactions of physiological disorders, such as diabetes,[31] and its sustained release,[32] immobilization,[7] and bioprobes[33] are of interest. Aluminum hydroxide and LDH have been individually used in the form of crystalline platelets as adsorbents for BSA molecules.[34−36] Preliminary results (not shown) of BSA adsorption using previously reported hierarchically porous LDHs[15] (prepared by ambient drying without the solvothermal treatment) lead to a negligible amount of protein
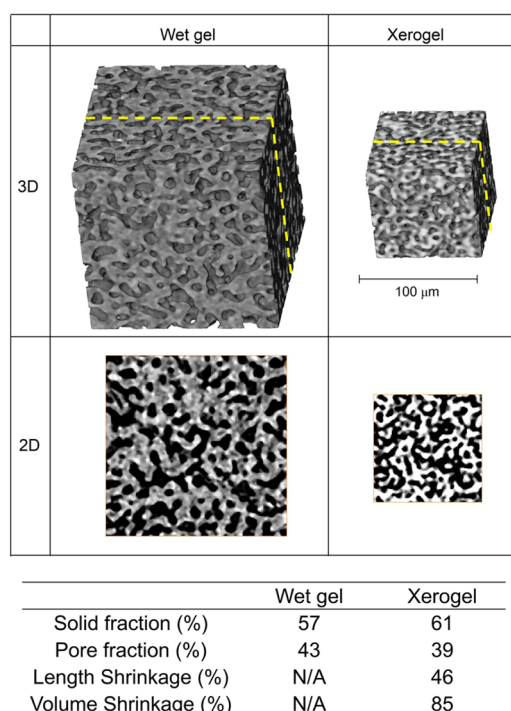
Figure 3. 3D and two-dimensional (2D) X-ray μ-CT images of the LDH–Alhy composites before (wet gel) and after (xerogel) drying at 300 K. The wet gel sample for μ-CT was prepared at Mg/Al = 0.3 and W_{PEO} = 0.03 g. Isotropic shrinkage took place during the drying, leading to the volume shrinkage of 85% and the linear shrinkage of 46%. Images were reconstructed from the same part of the monolithic sample. The yellow dotted lines in 3D images represent 2D planes shown as 2D images.

adsorption, where the mesopore size was too small to accommodate protein molecules and only macropores were available for protein adsorption; the surface area derived from macropores[37] is less than 10 m^2 g^{-1}.
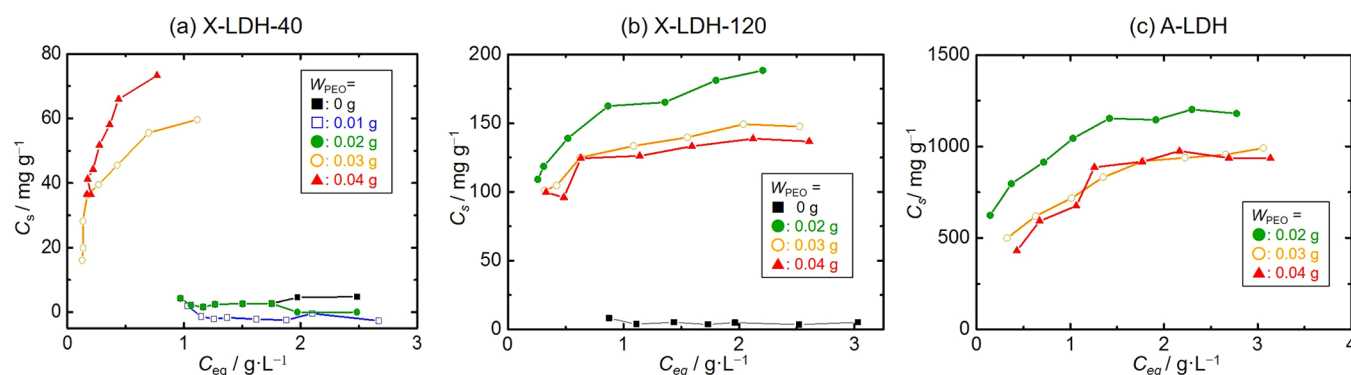
Figure 4a represents adsorption isotherms of BSA on X-LDH-40 at different W_{PEO}. At W_{PEO} = 0, 0.01, and 0.02 g, the adsorption of BSA was negligible. LDH–Alhy composites prepared at W_{PEO} = 0 and 0.01 g do not possess any macropores, limiting BSA adsorption to the external surface, where BSA adsorbed on the surface prevents further diffusion of protein through the mesopores into the bulk of the material. On the other hand, LDH–Alhy with a hierarchically porous structure (W_{PEO} = 0.03–0.04 g and macropore size = 1–2 μm)

shows much higher BSA loading as a result of the presence of co-continuous macropore channels for BSA molecules to diffuse through to the majority of the available surface. Corresponding adsorption isotherms of X-LDH-120 and A-LDH are plotted in panels b and c of Figure 4, respectively. As a result of the lack of realistic adsorption models for fitting the interactions between solid surfaces and proteins, many studies have reported the use of the Freundlich model as an approximative tool to evaluate and compare various solid/protein systems.[38] Freundlich adsorption isotherms for X-LDH-40, X-LDH-120, and A-LDH are represented in Figure S3 of the Supporting Information. The plots can be linearly fitted by eq 2, except for the case of X-LDH-40 at W_{PEO} = 0.02 g, whose microstructure is highly inhomogeneous because of structure deformation during drying. The K_f value increases in the order of X-LDH-40 < X-LDH-120 < A-LDH, as summarized in Table 2. The Freundlich constant, K_f of A-LDH prepared with W_{PEO}

Table 2. Summary of Freundlich Fitting of BSA Adsorption on Solid Surfaces

entry	W_{PEO}	K_f (mg g^{-1})	$1/n_f$	R^2
X-LDH-40	0.02	NA	NA	NA
	0.03	56	0.28	0.97
	0.04	86	0.41	0.95
X-LDH-120	0.02	158	0.24	0.96
	0.03	128	0.19	0.94
	0.04	121	0.17	0.78
A-LDH	0.02	996	0.23	0.97
	0.03	724	0.32	0.98
	0.04	676	0.40	0.85
Ref-LDH		70	0.32	0.93
Com-LDH		138	0.23	0.97

= 0.02 g is 996 mg g^{-1}. The value is 14 times that of Ref-LDH (70 mg g^{-1}), confirming that A-LDH composites prepared in the present study exhibit excellent adsorption properties compared to X-LDH, Ref-LDH, and Com-LDH. Clearly, the porous structure is the key factor that accounts for BSA loading, while other influences, slight pH change during adsorption and difference of hydroxylated surfaces, are negligible (Tables S1 and S2 of the Supporting Information). Indeed, while the surface of Ref-LDH with a higher ζ potential (+42 mV) should promote higher BSA adsorption than the LDH–Alhy composite (+37 mV for X-LDH-40), the reverse is observed;



Figure 4. BSA adsorption isotherms on (a) X-LDH-40, (b) X-LDH-120, and (c) A-LDH at 25 °C. Adsorption isotherms of BSA on A-LDH prepared at W_{PEO} = 0 and 0.01 g (without macropores) are not reproducible.

BSA has an isoelectric point of pI 4.7[39] and is negatively charged in the present adsorption condition (pH ~ 7).

Figure 5 shows plots of K_f values of LDH−Alhy composites against $S_{(>x\ nm)}$ that is a specific surface area obtained by
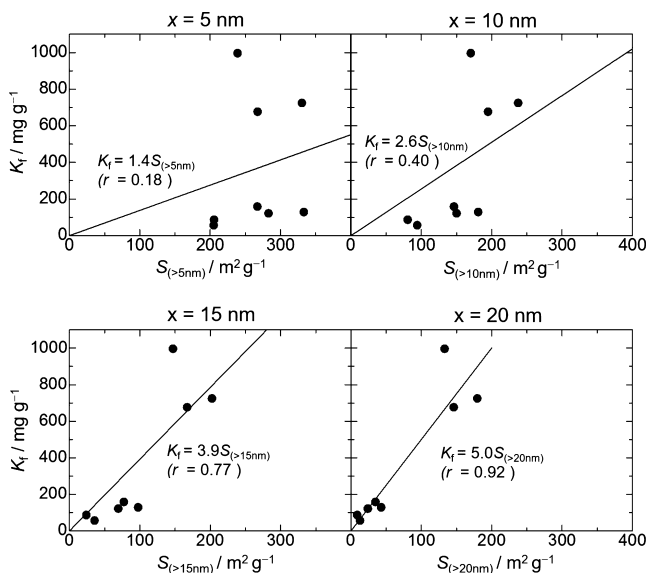
Figure 5. K_f versus $S_{(>x\ nm)}$ of LDH−Alhy composites. K_f values of LDH−Alhy composites listed in Table 2 are plotted. $S_{(>x\ nm)}$ = specific surface areas derived from the pores larger than x nm. The results of linear least squares fitting are depicted with the plots. r = correlation coefficient.

integrating surface areas derived from pores of $D_p > x$ nm; for example, $S_{(>5\ nm)}$ is a sum of surface areas derived from pores with a diameter of $D_p > 5$ nm. The LDH−Alhy composites prepared in the present study have tunable pore characteristics, and $S_{(>x\ nm)}$ was controllable to a large extent. Figure 5 shows K_f values against $S_{(>x\ nm)}$ for x = 5, 10, 15, and 20 nm pore size. K_f and $S_{(>5\ nm)}$ do not have correlation because relatively small mesopores cannot accommodate BSA. The surface area, which is derived from the mesopores whose sizes are insufficient for BSA adsorption, contributes less to $S_{(>x\ nm)}$ as the x value becomes larger. As a result, linear least squares fitting gives a better correlation coefficient r with an increasing x. At x = 15 and 20 nm, r was estimated as 0.77 and 0.92, respectively. These results reveal that D_p of ca. 20 nm is the threshold, which allows for the accommodation and adsorption of BSA molecules on the entire surfaces of mesopores. Although the pores of 10−20 nm are apparently larger than the size of BSA molecules ($5 \times 7 \times 7$ nm³), adsorption on the surface of these relatively small mesopores does not take place efficiently because the entrance of mesopores is blocked by the first few BSA molecules adsorbing there. This effect was indeed observed for X-LDH-40 (W_{PEO} = 0−0.02), in which mesopores ($D_{pm} < 15$ nm) in the absence of macropores exhibited negligible adsorption (Figure 4a). A similar size effect of mesopores on BSA adsorption was qualitatively reported on mesoporous silica, where SBA-15 with the pore diameter of 24 nm showed much better BSA adsorption than those with 3.8 and 7.7 nm in diameter.[40] The present results give very systematic and quantitative evidence for a threshold in the pore diameter for effective adsorption of BSA molecules to mesoporous materials. The approach demonstrated here will

be a promising platform to maximize S_{EFF} for respective proteins with different molecular sizes.

Ability for Encapsulation and Release of Immobilized Proteins. The capability of encapsulating immobilized protein and their sustained release are also an important feature for bioadsorbents. A previous study reported that BSA desorption from Zn−Al LDH took place by the addition of competitive anionic adsorbates.[41] Herein, HPO_4^{2-} and Cl^- ions were used as competitive ions to release pre-adsorbed BSA molecules. Table 3 summarizes the results of protein desorption from A-

**Table 3. Capability of Controllable Release of BSA from the LDH−Alhy Composite**

entry	releasing agent	releasing percentage (%)
A-LDH	HPO_4^{2-}	52
	Cl^-	1.8
	$HPO_4^{2-\ a}$	23
Com-LDH	HPO_4^{2-}	49
	Cl^-	1.1

^{a}BSA adsorbed on A-LDH was dried and immersed in an aqueous solution of releasing agent, HPO_4^{2-}.

LDH and Com-LDH. A total of 52% of BSA desorbed in 72 h from A-LDH in the case of using HPO_4^{2-} as a competitive anion, which is comparable to that from Com-LDH (49%). This result confirms that the protein desorption and adsorption take place with a large capacity for the present LDH−Alhy composites. Cl^- ions did not induce the desorption of BSA for both Com-LDH and A-LDH, which is due to the lower affinity of Cl^- and LDH surface and smaller negative charge compared to HPO_4^{2-}. While the LDH−Alhy composites (X-LDH and A-LDH) have a weight ratio of LDH/Alhy = 1:1, the desorption percentage by Cl^- of these composites is almost the same as pure LDH (~2%) (Table 3). A simple integration of respective surfaces of LDH and $Al(OH)_3$ cannot explain the low BSA desorption from the A-LDH composite observed with Cl^- as the counterion, because BSA desorption easily occurs on Alhy (50−60%) using Cl^- as a competitive ion. The unique surface texture of A-LDH, the nanomosaic surface composed of Alhy and LDH nanoparticles, would result in the peculiar restricted desorption, although further evidence is required. BSA molecules were also entrapped in the matrix of the composite by first immobilizing BSA within A-LDH, which was then dried to trap the protein within as the gel shrank. As summarized in Table 3 and Figure 6, the desorption of BSA molecules by HPO_4^{2-} from dried samples was <23%, which is less than half that of the non-dried sample of its original dimension (52%). These results demonstrate the possibilities of encapsulation and extended release of various protein molecules with a high capacity based on tunable hierarchically porous LDH. Combining LDH materials with various selectivities toward different molecules/ions will further open up biocompatible separation and purification required for biomedical applications.[42]

CONCLUSION

The preparation of biocompatible LDH−Alhy composites with an optimized S_{EFF} for large protein molecules is presented. S_{EFF} could be altered by the synthesis parameters, such as the amount of polymer additive and the drying conditions used. The capacity for protein loading was investigated with BSA as a model protein, which revealed the existence of a threshold on
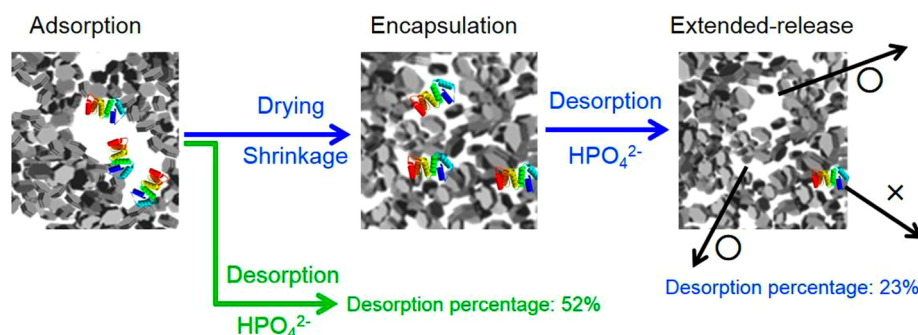
Figure 6. Schematic illustration showing the controllable release of BSA adsorbed on A-LDH.

the smaller critical mesopore size required to accommodate BSA molecules to be ca. $D_P = 20$ nm. Especially, the LDH−Alhy aerogel ($W_{PEO} = 0.02$ g) with a hierarchically porous structure and median mesopore size of 53.2 nm exhibited a remarkably high protein loading ($K_f = 996$ mg g^{-1}) when compared to Ref-LDH and Com-LDH standards. The BSA molecules pre-adsorbed on the composite were released by HPO_4^{2-} as a competitive adsorbate, while, when Cl$^-$ was the competing ion, BSA release was retarded to the extent comparable to pure LDH, presumably because of the unique surface texture, nanomosaic of LDH and Alhy. The tunable mesostructures in the range of nanometers to tens of nanometers are applicable to molecular sieving and purification of protein solutions. Further investigation based on this platform would open up many possibilities of using these hierarchically porous LDH−Alhy composites in various applications.

ASSOCIATED CONTENT

Ⓢ Supporting Information

The Supporting Information is available free of charge on the ACS Publications website at DOI: 10.1021/acs.langmuir.6b01925.

> N$_2$ sorption isotherms and BJH pore size distributions of LDH−Alhy and referential samples, linearized form of the adsorption isotherm according to the Freundlich model, influences of the heat drying temperature, pH, and sample mass on BSA adsorption, reproducibility of analysis based on the Freundlich equation, and influence of thermal treatment prior to N$_2$ adsorption measurements (PDF)

AUTHOR INFORMATION

Corresponding Author
*E-mail: tokudome@photomater.com.
Notes
The authors declare no competing financial interest.

ACKNOWLEDGMENTS

REFERENCES

(1) Mansur, H. S.; Lobato, Z. P.; Oréfice, R. L.; Vasconcelos, W. L.; Oliveira, C.; Machado, L. J. Surface Functionalization of Porous Glass Networks: Effects on Bovine Serum Albumin and Porcine Insulin Immobilization. *Biomacromolecules* **2000**, *1* (4), 789−797.

(2) Yuan, S. J.; Wan, D.; Liang, B.; Pehkonen, S. O.; Ting, Y. P.; Neoh, K. G.; Kang, E. T. Lysozyme-Coupled Poly(poly(ethylene glycol) methacrylate)-Stainless Steel Hybrids and Their Antifouling and Antibacterial Surfaces. *Langmuir* **2011**, *27* (6), 2761−2774.

(3) Zhu, L. P.; Jiang, J. H.; Zhu, B. K.; Xu, Y. Y. Immobilization of Bovine Serum Albumin onto Porous Polyethylene Membranes using Strongly Attached Polydopamine as a Spacer. *Colloids Surf., B* **2011**, *86* (1), 111−118.

(4) Guérard-Hélaine, C.; Légeret, B.; Fernandes, C.; Prévot, V.; Forano, C.; Lemaire, M. Efficient Immobilization of Fructose-6-Phosphate Aldolase in Layered Double Hydroxide: Improved Stereoselective Synthesis of Sugar Analogues. *New J. Chem.* **2011**, *35* (4), 776−779.

(5) An, Z.; Lu, S.; He, J.; Wang, Y. Colloidal Assembly of Proteins with Delaminated Lamellas of Layered Metal Hydroxide. *Langmuir* **2009**, *25* (18), 10704−10710.

(6) Mandal, H. S.; Kraatz, H. B. Effect of the Surface Curvature on the Secondary Structure of Peptides Adsorbed on Nanoparticles. *J. Am. Chem. Soc.* **2007**, *129* (20), 6356−6357.

(7) Roach, P.; Farrar, D.; Perry, C. C. Surface Tailoring for Controlled Protein Adsorption: Effect of Topography at the Nanometer Scale and Chemistry. *J. Am. Chem. Soc.* **2006**, *128* (12), 3939−3945.

(8) Charradi, K.; Forano, C.; Prevot, V.; Madern, D.; Ben Haj Amara, A.; Mousty, C. Characterization of Hemoglobin Immobilized in MgAl-Layered Double Hydroxides by the Coprecipitation Method. *Langmuir* **2010**, *26* (12), 9997−10004.

(9) Li, M.; Ji, H.; Wang, Y.; Liu, L.; Gao, F. MgFe-Layered Double Hydroxide Modified Electrodes for Direct Electron Transfer of Heme Proteins. *Biosens. Bioelectron.* **2012**, *38* (1), 239–244.

(10) Touisni, N.; Charmantray, F.; Helaine, V.; Forano, C.; Hecquet, L.; Mousty, C. Optimized Immobilization of Transketolase from *E. coli* in MgAl-Layered Double Hydroxides. *Colloids Surf., B* **2013**, *112*, 452–459.

(11) Shao, M.; Ning, F.; Zhao, J.; Wei, M.; Evans, D. G.; Duan, X. Preparation of $Fe_3O_4@SiO_2@$Layered Double Hydroxide Core–Shell Microspheres for Magnetic Separation of Proteins. *J. Am. Chem. Soc.* **2012**, *134* (2), 1071–1077.

(12) Wang, Q.; O'Hare, D. Recent Advances in the Synthesis and Application of Layered Double Hydroxide (LDH) Nanosheets. *Chem. Rev.* **2012**, *112* (7), 4124–4155.

(13) Guo, X. X.; Zhang, F. Z.; Evans, D. G.; Duan, X. Layered Double Hydroxide Films: Synthesis, Properties and Applications. *Chem. Commun.* **2010**, *46* (29), 5197–5210.

(14) Ni, X. M.; Kuang, K. Q.; Jin, X.; Xiao, X. K.; Liao, G. X. Large Scale Synthesis of Porous Microspheres of Mg-Al-Layerd Double Hydroxide with Improved Fire Suppression Effectiveness. *Solid State Sci.* **2010**, *12* (4), 546–551.

(15) Tokudome, Y.; Tarutani, N.; Nakanishi, K.; Takahashi, M. Layered Double Hydroxide (LDH)-based Monolith with Interconnected Hierarchical Channels: Enhanced Sorption Affinity for Anionic Species. *J. Mater. Chem. A* **2013**, *1* (26), 7702–7708.

(16) Tarutani, N.; Tokudome, Y.; Nakanishi, K.; Takahashi, M. Layered Double Hydroxide Composite Monoliths with Three-Dimensional Hierarchical Channels: Structural Control and Adsorption Behavior. *RSC Adv.* **2014**, *4* (31), 16075–16080.

(17) Touati, S.; Mansouri, H.; Bengueddach, A.; de Roy, A.; Forano, C.; Prevot, V. Nanostructured Layered Double Hydroxide Aerogels with Enhanced Adsorption Properties. *Chem. Commun.* **2012**, *48* (57), 7197–7199.

(18) Inacio, J.; Taviot-Gueho, C.; Forano, C.; Besse, J. P. Adsorption of MCPA Pesticide by MgAl-Layered Double Hydroxides. *Appl. Clay Sci.* **2001**, *18* (5–6), 255–264.

(19) Rau, C.; Wagner, U.; Pesic, Z.; De Fanis, A. Coherent Imaging at the Diamond Beamline I13. *Phys. Status Solidi A* **2011**, *208* (11), 2522–2525.

(20) Rockett, P.; Karagadde, S.; Guo, E.; Bent, J.; Hazekamp, J.; Kingsley, M.; Vila-Comamala, J.; Lee, P. D. A 4-D Dataset for Validation of Crystal Growth in a Complex Three-Phase Material, Ice Cream. *IOP Conf. Ser.: Mater. Sci. Eng.* **2015**, *84*, 012076.

(21) Atwood, R. C.; Bodey, A. J.; Price, S. W. T.; Basham, M.; Drakopoulos, M. A High-Throughput System for High-Quality Tomographic Reconstruction of Large Datasets at Diamond Light Source. *Philos. Trans. R. Soc., A* **2015**, *373* (2043), 20140398.

(22) Gash, A. E.; Tillotson, T. M.; Satcher, J. H.; Poco, J. F.; Hrubesh, L. W.; Simpson, R. L. Use of Epoxides in the Sol–Gel Synthesis of Porous Iron(III) Oxide Monoliths from Fe(III) Salts. *Chem. Mater.* **2001**, *13* (3), 999–1007.

(23) Oestreicher, V.; Jobbagy, M. One Pot Synthesis of Mg_2Al-$(OH)_6Cl·1.5H_2O$ Layered Double Hydroxides: The Epoxide Route. *Langmuir* **2013**, *29* (39), 12104–12109.

(24) Nakanishi, K. Pore Structure Control of Silica Gels Based on Phase Separation. *J. Porous Mater.* **1997**, *4* (2), 67–112.

(25) Roussel, H.; Briois, V.; Elkaim, E.; de Roy, A.; Besse, J. P. Cationic Order and Structure of [Zn–Cr–Cl] and [Cu–Cr–Cl] Layered Double Hydroxides: A XRD and EXAPS study. *J. Phys. Chem. B* **2000**, *104* (25), 5915–5923.

(26) Kreuter, J. Nanoparticle-Based Drug Delivery Systems. *J. Controlled Release* **1991**, *16* (1–2), 169–176.

(27) Kanamori, K.; Kodera, Y.; Hayase, G.; Nakanishi, K.; Hanada, T. Transition from Transparent Aerogels to Hierarchically Porous Monoliths in Polymethylsilsesquioxane Sol–Gel System. *J. Colloid Interface Sci.* **2011**, *357* (2), 336–344.

(28) Brinker, C. J.; Scherer, G. W. *Sol–Gel Science: The Physics and Chemistry of Sol–Gel Processing*; Academic Press: San Diego, CA, 1990.

(29) Leggio, C.; Galantini, L.; Konarev, P. V.; Pavel, N. V. Urea-Induced Denaturation Process on Defatted Human Serum Albumin and in the Presence of Palmitic Acid. *J. Phys. Chem. B* **2009**, *113* (37), 12590–12602.

(30) He, X. M.; Carter, D. C. Atomic-Structure and Chemistry of Human Serum-Albumin. *Nature* **1992**, *358* (6383), 209–215.

(31) Reddy, S.; Bichler, J.; Wellsknecht, K. J.; Thorpe, S. R.; Baynes, J. W. N-ε-(Carboxymethyl)Lysine Is a Dominant Advanced Glycation End-Product (AGE) Antigen in Tissue Proteins. *Biochemistry* **1995**, *34* (34), 10872–10878.

(32) Calvo, P.; RemunanLopez, C.; VilaJato, J. L.; Alonso, M. J. Novel Hydrophilic Chitosan-Polyethylene Oxide Nanoparticles as Protein Carriers. *J. Appl. Polym. Sci.* **1997**, *63* (1), 125–132.

(33) Qin, W.; Ding, D.; Liu, J. Z.; Yuan, W. Z.; Hu, Y.; Liu, B.; Tang, B. Z. Biocompatible Nanoparticles with Aggregation-Induced Emission Characteristics as Far-Red/Near-Infrared Fluorescent Bioprobes for In Vitro and In Vivo Imaging Applications. *Adv. Funct. Mater.* **2012**, *22* (4), 771–779.

(34) Monash, P.; Majhi, A.; Pugazhenthi, G. Separation of Bovine Serum Albumin (BSA) Using γ-Al_2O_3–Clay Composite Ultrafiltration Membrane. *J. Chem. Technol. Biotechnol.* **2010**, *85* (4), 545–554.

(35) Chao, V. W. K.; Hsu, C. C.; Lu, W. M.; Chen, W. J.; Naveen, B.; Tsai, T. Y. Protein-Concentration-Dependent Adsorption Behaviour of Inorganic Layered Materials. *RSC Adv.* **2015**, *5* (15), 10936–10943.

(36) Gu, Z.; Zuo, H. L.; Li, L.; Wu, A. H.; Xu, Z. P. Pre-Coating Layered Double Hydroxide Nanoparticles with Albumin to Improve Colloidal Stability and Cellular Uptake. *J. Mater. Chem. B* **2015**, *3* (16), 3331–3339.

(37) Tokudome, Y.; Nakanishi, K.; Kosaka, S.; Kariya, A.; Kaji, H.; Hanada, T. Synthesis of High-Silica and Low-Silica Zeolite Monoliths with Trimodal Pores. *Microporous Mesoporous Mater.* **2010**, *132* (3), 538–542.

(38) Prevot, V.; Mousy, C.; Forano, C. State of the Art in Biomolecule and Layered Double Hydroxide Assemblies. In *Advances in Chemistry Research*; Taylor, J. C., Ed.; Nova Scientific Publishers: Hauppauge, NY, 2012; Vol. 17, pp 35–84.

(39) Chun, K. Y.; Stroeve, P. Protein Transport in Nanoporous Membranes Modified with Self-Assembled Monolayers of Functionalized Thiols. *Langmuir* **2002**, *18* (12), 4653–4658.

(40) Katiyar, A.; Ji, L.; Smirniotis, P.; Pinto, N. G. Protein Adsorption on the Mesoporous Molecular Sieve Silicate SBA-15: Effects of pH and Pore Size. *J. Chromatogr. A* **2005**, *1069* (1), 119–126.

(41) Zhang, T.; Zhou, Y. M.; He, M.; Zhu, Y. X.; Bu, X. H.; Wang, Y. J. Biomimetic Fabrication of Hierarchically Structured LDHs/ZnO Composites for the Separation of Bovine Serum Albumin. *Chem. Eng. J.* **2013**, *219*, 278–285.

(42) Ma, W.; Lv, T. F.; Song, X. Y.; Cheng, Z. H.; Duan, S. B.; Xin, G.; Liu, F. J.; Pan, D. C. Characteristics of Selective Fluoride Adsorption by Biocarbon–Mg/Al Layered Double Hydroxides Composites from Protein Solutions: Kinetics and Equilibrium Isotherms Study. *J. Hazard. Mater.* **2014**, *268*, 166–176.